Time-averaged second-order pressure and velocity measurements in a pressurized oscillating flow prime mover

Richard Paridaens, Smaine Kouidri, Fathi Jebali Jerbi

Time-averaged second-order pressure and velocity measurements in a pressurized oscillating flow prime mover †

Richard Paridaens[1,*], Smaine Kouidri[2,3] and Fathi Jebali Jerbi[2,3]

[1]*DynFluid, Arts et Métiers, 151 boulevard de l'Hôpital, 75013 Paris, France*
[2]*LIMSI-CNRS, BP 133-91403 Orsay Cedex, France*
[3]*UPMC Univ Paris 06, UFR 919, 4 place Jussieu, 75752 Paris Cedex 05, France*

Abstract

Nonlinear phenomena in oscillating flow devices cause the appearance of a relatively minor secondary flow known as acoustic streaming, which is superimposed on the primary oscillating flow. Knowledge of control parameters, such as the time-averaged second-order velocity and pressure, would elucidate the non-linear phenomena responsible for this part of the decrease in the system's energetic efficiency. This paper focuses on the characterization of a travelling wave oscillating flow engine by measuring the time-averaged second-order pressure and velocity. Laser Doppler Velocimetry technique was used to measure the time-averaged second-order velocity. As streaming is a second-order phenomenon, its measurement requires specific settings especially in a pressurized device. Difficulties in obtaining the proper settings are highlighted in this study. The experiments were performed for mean pressures varying from 10 bars to 22 bars. Non-linear effect does not constantly increase with pressure.

Keywords: LDV measurement; Oscillating flow; Streaming; Time-averaged second-order pressure; Time-averaged second-order velocity

1. Introduction

Oscillating flow prime mover is an energy conversion system that can convert thermal energy to acoustic energy. This system uses non-polluting fluids, nitrogen, helium or air, and is of interest to researchers. Most oscillating flow machines designed for high energy performance have shown a coefficient of performance of about 20% of the Carnot coefficient [1]. Few devices [2-4] have achieved a coefficient of performance of 41%–49% of the Carnot coefficient. Backhaus and Swift [2, 3] designed and built a new type thermoacoustic engine based on travelling waves. At its most efficient operating point, the author succeeded in obtaining an efficiency of 41% of the Carnot efficiency. By using a similar type thermoacoustic engine, Tijani and Spoelstra [4] achieved a record performance of 49% of the Carnot efficiency.

Low energy efficiencies are related to the multiplicity and complexity of the underlying physical phenomena. Combination of acoustic, thermal, and thermodynamic phenomena [5, 6] complicates the understanding and control of these energy conversion systems. The main obstacle to their development and the reason for their low energy efficiency is now a central concern of the oscillating flow community [7-11]. To improve this situation, all sources of energy losses must be identified and reduced. Acoustic streaming, a secondary flow superimposed on the first-order oscillating flow, has been identified as one of the major sources of energy dissipation in oscillating flow devices [12-14]. It is generated by non-linear propagation of the high amplitude waves occurring in an oscillating flow system. From energy considerations and despite its low level, this second-order phenomenon constitutes an undesirable loss mechanism. Acoustic streaming was observed for the first time in 1831 by Faraday [15].

After this above-mentioned observation, numerous investigations have been conducted. Early studies were mainly theoretical. The first theoretical description of acoustic streaming appeared in 1884 [16]. Lord Rayleigh found an analytical solution describing the phenomenon in large channels subjected to acoustic standing waves. Subsequently, many theoretical solutions have been proposed [17, 18]. Experimental investigations on acoustic streaming emerged subsequently. After the first observation was made by Faraday [15], the second experimental study appeared only a century later. In 1931, Andrade [19] investigated the pattern of acoustic streaming generated by standing waves in a cylindrical resonator. The pattern of the secondary flow observed by Andrade was in agreement with the pattern obtained by Rayleigh's analytical

*Corresponding author. Tel.: +33 609978376, Fax.: +33 1 44246411
E-mail address: richard.paridaens@ensam.eu

model.

Experimental investigations of acoustic streaming, which were qualitative initially, became increasingly quantitative with the development of laser measurement techniques, such as Particle Image Velocimetry (PIV) and Laser Doppler Velocimetry (LDV). The first quantitative investigation of acoustic streaming was conducted by Arroyo and Greated [20] in 1991. They measured the three components of acoustic streaming velocity by PIV in a rectangular resonator subjected to acoustic standing waves. Experimental results were compared with Rayleigh's theoretical results, and a satisfactory agreement was observed.

Thompson and Atchley [21] obtained good agreement between Rayleigh's theory and their measurements. Their measurements of acoustic streaming velocity were performed by using LDV in a circular section resonator. Subsequently, Thompson et al. [22] investigated the influence of three temperature boundary conditions on the behavior of the acoustic streaming velocity. They imposed three different temperature conditions on the resonator, as follows: isothermal, insulated, and uncontrolled. The uncontrolled condition means that no special disposition was made. For the insulated and uncontrolled configurations, they observed that the acoustic streaming reached its steady state after 15 min to 35 min. In steady state, they observed the existence of a temperature gradient along the resonator tube for the two configurations. To investigate the influence of the temperature gradient on the acoustic streaming, they switched off the loudspeaker and then turned it on long enough to make the secondary flow disappear but short enough to maintain the temperature gradient. Then, they measured the acoustic streaming velocity and observed that the values obtained matched the steady state values. Therefore, they deduced that the transition state of acoustic streaming was due to the establishment of the temperature gradient.

Moreau et al. [23] were the first to measure the inner vortex described by analytical models. Their investigation focused on the influence of the non-linear Reynolds number on the shape of the inner and outer vortices. They compared the transverse profiles of the acoustic streaming velocity for different values of the non-linear Reynolds number (R_{nl}) between 1 and 247. When the Reynolds number increased, i.e., the inertial forces increased, the measured streaming velocity decreased, deviating from the theoretical values.

Moreau et al. [24] also investigated the effect of the stack on acoustic streaming. They measured the axial profile of the acoustic streaming velocity in the center of the resonator by LDV. The measurements were performed, first of all, without stack and the authors observed a classical structure with Rayleigh vortex. They introduced a stack in the resonator and observed that the structure of Rayleigh vortex was not affected. The streaming velocity field was modified only in the vicinity of the stack. The major perturbations occurred when the stack was located near the maximum velocity.

All above-described experimental investigations on acoustic streaming were for standing waves. There have been few experimental studies on the acoustic streaming generated by progressive waves. In this area, the investigation performed by Desjouy et al. [25] can be cited. They measured the acoustic streaming velocity in an annular loop. The acoustic waves within the system were generated by two loudspeakers. The phase control of the loudspeakers allowed for the selection of the wave type (standing or progressive). When the system operated with standing waves, a classical structure with Rayleigh vortex is observed. The axial profile of the acoustic streaming velocity was sinusoidal. The streaming velocity nodes were located at the position of the acoustic velocity nodes and anodes. When the device operated with progressive waves, the axial profile lost its sinusoidal form and became uniform. In agreement with their theoretical results, the authors observed that the measured velocity was oriented toward the opposite side of the propagation direction of the acoustic waves.

Many investigations on acoustic streaming have focused on resonant systems. Acoustic streaming has been little studied in oscillating flow devices. Among the experimental studies, the investigation of Biwa et al. [26] and the investigation of Debesse [27] can be cited.

Biwa et al. [26] studied the effect of a jet pump on the acoustic streaming. The role of a jet pump is to minimize the mass flow circulating in a system loop [2]. The authors measured the axial profile of the acoustic streaming velocity in the loop of an oscillating flow engine for two different positions of the jet pump. The pump was placed first in one direction, and subsequently, in the other direction. The profile of the streaming velocity was totally modified by the direction of the jet pump. Biwa et al. [26] highlighted the importance of the jet pump on the secondary flow.

Debesse [27] measured the acoustic streaming velocity by PIV in a standing wave oscillating flow engine pressurized to 20 bars. He measured the streaming velocity and observed recirculation cells with different shapes compared with those predicted by the theoretical models. To explain the difference between the theoretical and experimental results, Debesse hypothesized the existence of a third type of flow. To verify this hypothesis, measurements were obtained immediately after the oscillating flow device was turned off and in the absence of acoustic waves. In this configuration, he observed a residual flow with a velocity an order of magnitude smaller than the acoustic streaming velocity. According to Debesse, this flow could be due to a thermoconvective phenomenon and could be the reason for the breakdown of the recirculation cells.

Heat losses between the two exchangers are due to the axial velocity. Thus, the experimental studies on acoustic streaming have mostly focused on this parameter. However, this non-linear phenomenon is also characterized by its excess pressure, called the time-averaged second-order pressure. This variable has not been investigated much experimentally. Smith and Swift [28] investigated this pressure in an acoustic device subjected to standing waves. This quantity is small. Thus, the

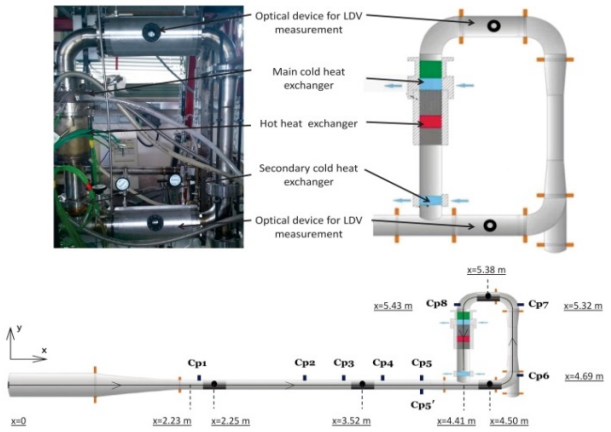

Fig. 1. Oscillating flow prime mover.

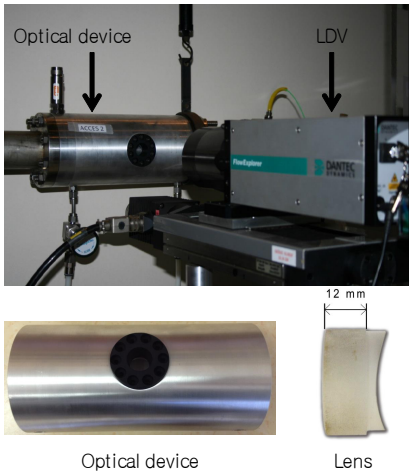

Fig. 2. Measurements of velocities by LDV in the oscillating flow prime mover.

authors focused their attention on the accuracy of the sensors. To minimize the linearity error of the sensor, they used a polynomial function of order 3. Then, the longitudinal profile of the time-averaged second-order pressure is measured along the resonator. Good compliance with the theory is obtained. The antinodes of the time-averaged second-order pressure corresponded to the nodes of the acoustic pressure.

Acoustic streaming has been little investigated in an oscillating flow engine. Major investigations have focused on the axial streaming velocity, to the detriment of the time-averaged second-order pressure. Bboth the time-averaged second-order axial velocity and pressure were measured in a pressurized travelling wave oscillating flow engine. The behavior of the streaming under variation of the mean pressure is also studied.

2. Experimental set-up

The experimental apparatus is an oscillating flow prime mover composed of a closed loop and a 4.25 m long resonator. The length of the system leads to acoustic waves with a frequency of 22 Hz. The active part of the system in which the energy conversion is made is located in the loop. The temperature of the heat exchanger is produced by the Joule effect and can reach 930 K. The temperature of the cold exchanger was maintained by the circulation of tap water. The device was filled with nitrogen and can operate up to a mean pressure of 30 bars. Acoustic waves appear only 14 min after the ignition of the engine. The steady state is reached after 78 min. In this case, the authors chose to define the steady state when the acoustic pressure amplitude has a variation of less than 1%. The measurements of the acoustic pressure and the time-averaged second-order pressure were obtained during the steady state by Kistler 701A piezoelectric pressure sensors flush mounted on the travelling wave engine at the positions *Cp1* to *Cp8* (Fig. 1). This sensor has a calibrated partial range from 0 to 2.5 bars and is able to withstand pressure up to 400 bars. Its linearity is lower than 0.5% of the full scale output.

The measurements of acoustic and streaming velocities were performed by LDV (Fig. 2). To visualize the flow, this

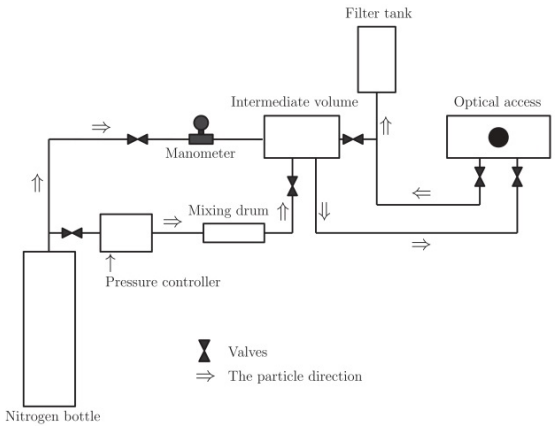

Fig. 3. Seeding system.

non-intrusive method needs an optical device and a seeding system. The optical device is composed of a cylindrical tube on which a lens is flush mounted. It was designed to resist pressures up to 40 bars.

To seed in a pressurized device, a specific system is required. In fact, the seeding pressure has to be higher than the operating pressure. The seeding system used in this investigation is composed of a nitrogen bottle, a pressure controller, a mixing drum, an intermediate volume, a manometer and a filter tank. Magnesium oxide powder is used for the seeding particles. Silicon dioxide (1%) was mixed with the magnesium oxide powder to reduce the risk of aggregation. Placed in the mixing drum, the particles were ready to be seeded into the device. As shown in Fig. 3, the seeding circuit was composed of primary and secondary circuits. Both circuits link the nitrogen bottle to the intermediate volume. The primary circuit is composed of two valves, the pressure controller, and the mixing drum. The secondary circuit is composed of a valve and the manometer. As the mixing drum does not resist a mean pressure over 10 bars, the primary circuit is limited to that pressure level. The secondary circuit and the intermediate

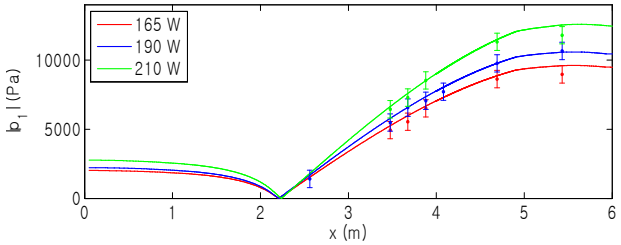

Fig. 4. Distribution of acoustic pressure for a mean pressure of 14 bars for three heat powers, as follows: 165, 190 and 210 W.

volume allow seeding at a pressure higher than 10 bars. Seeding the particles into the device is done in two steps. During the first step, the drum delivers an appropriate amount of powder to the intermediate volume. Then, the particles are seeded by the second circuit into the system via the optical devices. Seeding is performed locally to avoid the risk of obstructing the regenerator. As the connectors used for the secondary circuit are limited to pressures up to 20 bars, the measurements performed by LDV in the device do not exceed a mean pressure of 18 bars. The filter tank is linked to the optical access and to the intermediate volume to evacuate the particles at the end of the experiment.

3. Experimental results

This section presents the results of the measurements performed in the oscillating flow prime mover. Inside the device, each time and space dependent variable *F(x,t)* can be written as a function of its order [2], as follows:

$$F(x,t) = F_m + R_e\left[F_1 e^{i\omega t}\right] + F_{2,0} + R_e\left[F_{2,2} e^{i\omega t}\right] + \ldots \quad (1)$$

F_m is the mean value that exists in the absence of any acoustic wave. The subscript "1" represents the first order term and the subscript "*2*" the second-order term. "*2,0*" and "*2,2*" respectively represent the independent time term and the time-dependent term of the second order.

3.1 Acoustic fields

The streaming is generated by the acoustic wave. Thus, the acoustic fields were investigated first. The results of the measurements of the acoustic pressure and velocity are presented in this section. Fig. 4 shows the acoustic pressure distribution ($|p_1|$) along the device for a mean pressure (p_0) of 14 bars for three heat powers 165, 190 and 210 W. The theoretical acoustic pressure numerically calculated by DeltaEC [29] matches the experimental data well. The relative errors are less than 6%. As the pressure nodes depend only on the geometric configuration, they were located at the position x = 2.23 m regardless of the mean pressures and the heat powers.

To investigate the effect of the mean pressure, the distributions of the acoustic pressure versus the mean pressure for the *Cp3* sensor and for several heat powers are plotted in Fig. 5.

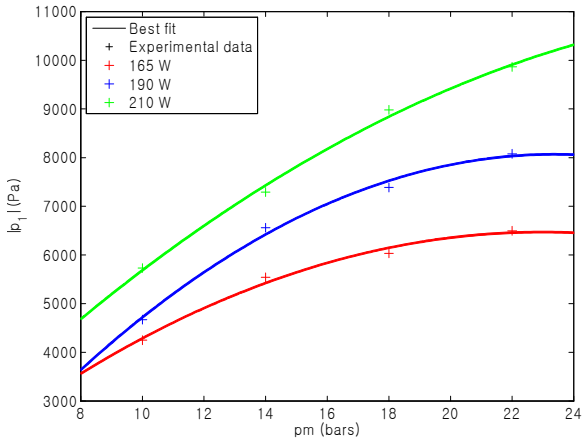

Fig. 5. Acoustic pressure versus mean pressure for the pressure sensor Cp3.

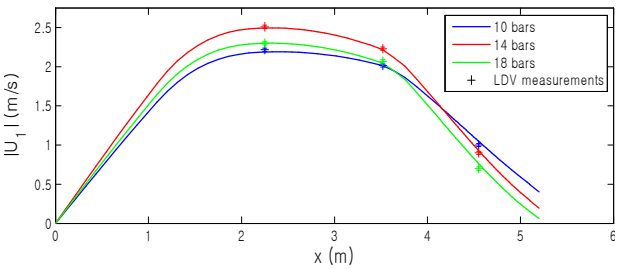

Fig. 6. Amplitude of acoustic velocities versus *x* for a heat power of 165 W and three mean pressures, as follows: 10, 14 and 18 bars.

These curves show that for each heat power, p_1 tends to increase parabolically with the mean pressure. The measurement of the acoustic pressure versus the mean pressure was limited to a mean pressure of 22 bars because the acoustic pressure amplitude did not reach a stable value for higher pressures.

Fig. 6 represents the axial profiles of the acoustic velocity ($|u_1|$) at the centerline of the duct for a heat power of 165 W and three different mean pressures, as follows: 10, 14 and 18 bars. The lines represent the theory, and the dots represent the measurements performed by LDV. The LDV measurement has been performed through the optical devices in the resonator at the positions $x = 2.25\ m$ and $x = 3.52\ m$ and in the closed loop at the position $x = 4.50\ m$. To obtain the experimental data, the signal was processed in accordance with the method described by Moreau et al. [23]. Good agreement was observed between the theoretical and the experimental values.

3.2 Acoustic streaming

After the experimental investigation of the acoustic fields, measurements of the acoustic streaming were obtained. However, to measure the streaming velocity in accordance with the method described by Moreau et al. [23], specific settings are required. Fig. 7, which represents the axial streaming velocity versus the number of samples, shows the criterion for obtaining an accurate measurement. To enhance the criterion, the

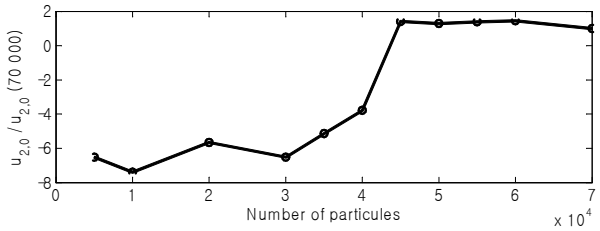

Fig. 7. The streaming velocity versus the number of samples.

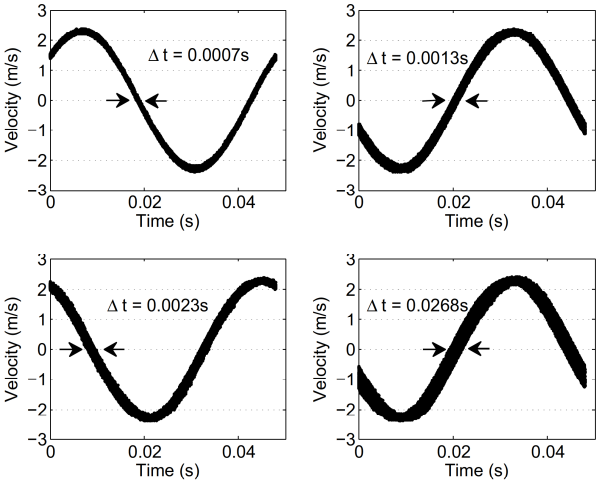

Fig. 8. The thickness of the curve, a setting parameter.

streaming velocities are normalized by the value obtained for a number of samples equal to 70000. In this configuration, particles less than 45000 provide an incorrect value. The value of the streaming velocity was stable and is considered as appropriate only for a number of particles higher than 45000. This result is in agreement with that obtained by Moreau et al. [23]. The measured velocities presented later in this article have been obtained for a number of particles equal to 50000.

The second important parameter to set is the time acquisition. This parameter, as shown in Fig. 8, affected the thickness of the processed signal. Thickness increases with the time acquisition. The influence of the thickness on the measured streaming velocity has been investigated. Its evolution versus Δt/T is represented in Fig. 9. Δt is the thickness, and T is the signal period. As the correct value is assumed to be obtained for the smallest thickness, the velocities are normalized by the value acquired at Δt/ T = 1.4%. Fig. 9 shows that the streaming velocity depends strongly on this parameter. When Δt/T is higher than 4%, the streaming velocity deviates by 63% from its initial value. When it is smaller than 4%, the relative error is less than 5%. To obtain correct values of the streaming velocity, each measurement needs to have a Δt/T smaller than 4%. Under our conditions, an acquisition time of less than 30 s provides a signal with a Δt/T smaller than 4%. Thus, the maximum acquisition time is set equal to 30 s.

To obtain an accurate measurement of the streaming velocity, the acquisition time has to be less than 30 s and the number of particles has to be higher than 45000. However, these parameters are not independent. They are linked by a proportional relationship, as follows:

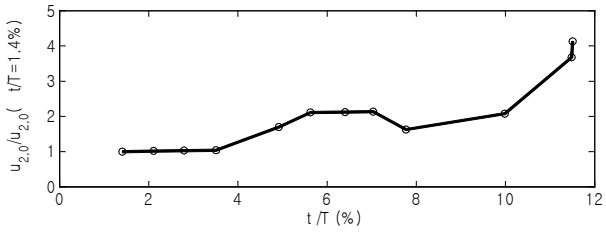

Fig. 9. Measurements of streaming velocities versus *Δt/T*.

$$Fa_{average} = \frac{Particles\_number}{Acquisition\_time} \tag{2}$$

$Fa_{average}$ is the average data rate. It is defined as follows:

$$Fa_{average} = \frac{1}{T}\int_0^{Acquisition\_time} Fa.dt \tag{3}$$

Fa is the data rate, and *T* is the period of the acoustic wave. This parameter cannot be adjusted. It depends on external conditions such as the seeding and the flow. The link between the two parameters makes their simultaneous adjustment difficult. As shown in Eqs. (2) and (3), higher data rate leads to the easy achievement of a large number of particles for a short time acquisition. However, in the present configuration, the data rate decreases quickly after seeding. Moreover, this decrease is accentuated by the increase of the mean pressure.

Despite this difficulty, the measurement of the acoustic streaming velocity ($u_{2,0}$) has been performed in the resonator and in the closed loop for a heat power of 165 W and three different mean pressures, as follows: 10, 14 and 18 bars. The radial profiles are represented for $x = 3.52\ m$ in Fig. 10. η is the adimensional radial coordinate. The theoretical values represented by the lines were calculated using the model of Paridaens et al. [30]. Good agreement was obtained between the theory and the measurements, except in the vicinity of the wall. The difference near the wall could come from the theory because the model neglects the effect of the curvature of the wall. It could also come from the measurement because the seeding particles may not correctly follow the flow near the wall. At the line center, the streaming velocity is negative, which means that the velocity is oriented toward the pressure node located at $x = 2.23\ m$. This result is in agreement with the result obtained by Hamilton et al. [31].

Fig. 11 represents the LDV measurements of the acoustic streaming velocities in the closed loop for $x = 4.50\ m$. The measurements have been realized for a heat power of 165 W for three different mean pressures (10, 14 and 18 bars). As the measurement of the second order velocity in the closed loop is more difficult to perform than in the resonator, fewer points

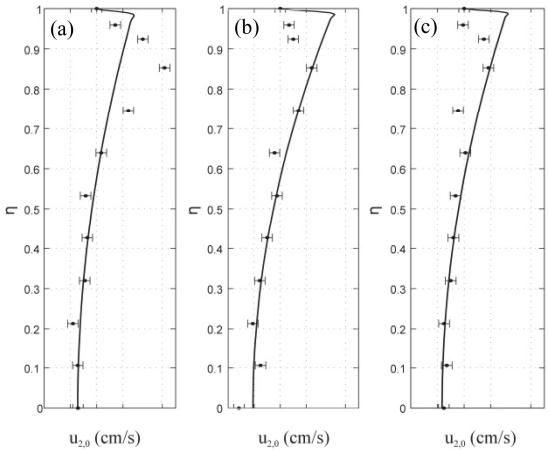

Fig. 10. Acoustic streaming velocity proles in the resonator for x = *3.52 m* for a heat power of 165 W and three different mean pressures: (a) 10 bars; (b) 14 bars; (c) 18 bars.

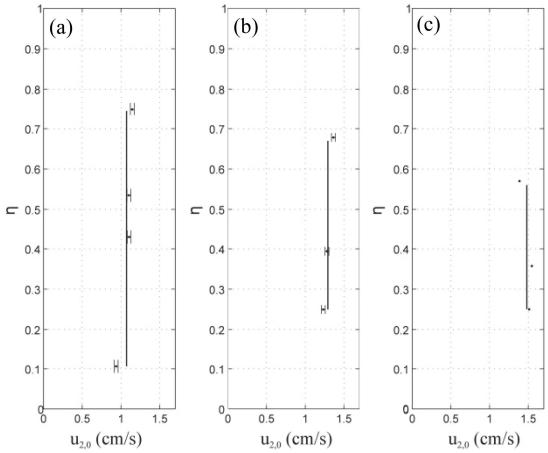

Fig. 11. Acoustic streaming velocity profiles in the closed loop for x = *4.50 m* for a heat power of 165 W and three different mean pressures: (a) 10 bars; (b) 14 bars; (c) 18 bars.

are represented on Fig. 11 compared to Fig. 10. It is not easy to obtain a proper measurement of the streaming velocity, since the mass flow circulates in the closed loop [12]. This mass flow would carry away the seeding particles from the measurement volume. As the measurements seem to not vary with η, the average values are represented in a full line. On Fig. 6, the values of the acoustic velocities are lower in the closed loop than in the resonator. This result could explain the higher values of the streaming velocities on Fig. 10 compared with those on Fig. 11. However, although the acoustic velocity is higher for 14 bars than for 18 bars (Fig. 6), the same result is not observed for the streaming velocity, neither in the closed loop nor in the resonator. In the device, the streaming velocities increase when the average pressure increases from 10 bars to 18 bars. Thus, the average pressure seems to be an influential parameter on the acoustic streaming. It would have been interesting to further investigate the effect of the mean pressure on the acoustic streaming velocity. Unfortunately, this investigation could not be conducted for two reasons. The first reason is the accuracy of the mean pressure measurement. Its measurement has only an accuracy of 0.8 bar because of the disturbance related to the particle injection. The second reason is the seeding device. It could not exceed a pressure injection higher than 20 bars. Thus, the measurements were performed only at lower pressures.

However, as the time-averaged second-order pressure ($p_{2,0}$) also characterizes the streaming phenomenon and does not require seed particles [32], the effect of the mean pressure on the acoustic streaming could be conducted via this parameter. As the standing wave ratio is higher than 98% in the resonator, the measurement method used by Smith and Swift [28] is applied to obtain the time-averaged second-order pressure in the oscillating flow device. A polynomial law of order three is used to minimize the error because of the non-linearity of the pressure sensor and to obtain a high accuracy. Before investigating the effect of the mean pressure on the time-averaged

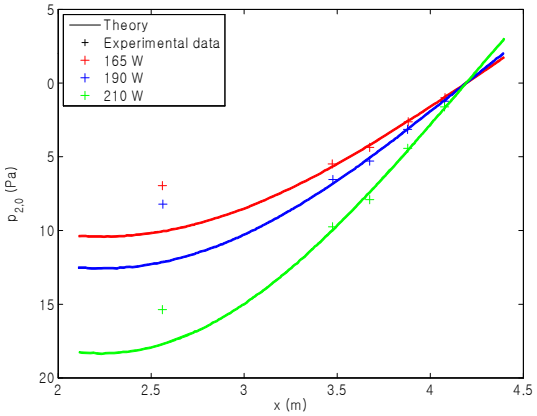

Fig. 12. Time-averaged second-order pressure distribution for mean pressure of 14 bars.

second-order pressure, its distribution along the resonator is plotted in Fig. 12 for a mean pressure of 14 bars and three heat powers, as follows: 165, 190 and 210 W. The lines and the dots represent the theoretical and the experimental values, respectively. The experimental results match the theoretical ones quite well. The location of the pressure node, at the left side of the curve, explains the discrepancies observed for the sensor Cp1. The relative error between theory and experiment is approximately 6%. The distributions of the time-averaged second-order pressure have the same form as the ones measured by Smith and Swift. Moreover, the minimum pressure is reached at the position of the acoustic pressure node.

As the measurement of the time-averaged second-order pressure was validated by the theory, the effect of the mean pressure could be conducted on it. Its evolutions, normalized by its minimum $|p_{2,0min}|$, versus the mean pressure are shown in Fig. 13. The evolutions of the time-averaged second-order pressure are parabolic and do not depend on the position. For each sensor, this variable characteristic of the non-linear effects reaches a maximum value for a mean pressure of 17 bars.

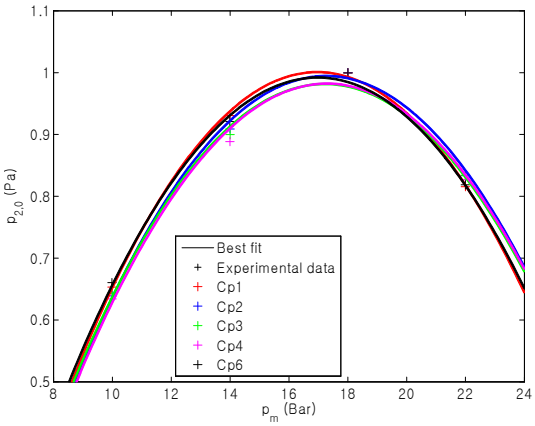

Fig. 13. Time-averaged second-order pressure versus mean pressure for a heat power of 165 W.

For the streaming velocity (Figs. 10 and 11), an increase of the mean pressure from 10 to 18 bars generates an increase of the time-averaged second-order pressure. The evolution of this pressure could be explained by two antagonistic effects. In fact, the time-averaged second-order pressure could be expressed by the following relationship [28]:

$$p_{2,0} \propto \frac{|p_1|}{\rho_m} \tag{1}$$

In the evolution of $|p_1|$ versus p_m shown in Fig. 5, the time-averaged second-order pressure tends to increase when the mean pressure increases. However, when the mean pressure increases, the density increases, thereby amplifying the inertial effects. As shown by Moreau et al. [23], the inertial effects tend to reduce the streaming phenomenon. Furthermore, a decrease of the streaming phenomenon could also be seen in Eq. (4).

3. Conclusion

An experimental investigation of the acoustic streaming phenomenon has been conducted in a pressurized travelling wave oscillating flow engine. To measure this phenomenon, specific settings are required. To measure the velocity, the number of acquired particles and the time acquisition need to be adjusted precisely. As these two parameters are not independent, and the oscillating flow device is under pressure, the parameters are not easily adjusted. For the time-averaged second-order pressure, a specific house calibration has been performed, and a polynomial law of order three has been used to minimize the errors because of the non-linearity. The experimental pressure and velocity are compared with the theoretical values, and a good agreement is observed. Because the measurement of the streaming velocity is limited by the seeding system, the influence of the mean pressure on the acoustic streaming has been investigated on a large range for the time-averaged second-order pressure. In the present configuration, a maximum pressure was obtained for a mean pressure of 17 bars regardless of the location in the resonator. Understanding the behavior of acoustic streaming in an oscillating flow system is an important step in reducing this phenomenon and in increasing the efficiency of oscillating flow devices.

Nomenclature

Cp_i	: Position of the piezoelectric pressure sensors; i varying from 1 to 8
$F(x,t)$	: Time and space dependent variable
F_m	: Mean value of the variable F(x,t) in absence of any acoustic wave
F_1	: First order term of the variable F(x,t)
$F_{2,0}$	: Time-averaged second-order of the variable F(x,t)
$F_{2,2}$	: Time-dependent second order of the variable F(x,t)
p_1	: Acoustic pressure [Pa]
$\|p_1\|$	: Amplitude of the acoustic pressure [Pa]
p_0	: Mean pressure [bar]
$p_{2,0}$	: Time-averaged second-order pressure [Pa]
u_1	: Acoustic velocity [m/s]
$\|u_1\|$	: Amplitude of the acoustic velocity [m/s]
$u_{2,0}$	: Time-averaged second-order velocity [m/s]
x	: Axial coordinate [m]
T	: Period of the acoustic wave [s]
η	: Adimensional radial coordinate
Δt	: Thickness of the measured signal [s]
ω	: Angular frequency of the acoustic wave [rad/s]
ρ_m	: Mean density in absence of any acoustic wave [kg/m^3]

References

[1] K. Godshalk, C. Jin, Y. Kwong, E. Hershberg, G. Swift, R. Radebaugh, C. S. Kim, K. S. Hong and M. K. Kim, Characterization of 350 Hz thermoacoustic driven orifice pulse tube refrigerator with measurements of the phase of the mass flow and pressure, *Advances in cryogenic*, 41 (1996) 1411-1418.

[2] S. Backhaus and G. W. Swift, A thermoacoustic-stirling heat engine: Detailed study, *Journal of the Acoustical Society of America*, 107 (2000) 3148-3166.

[3] S. Backhaus and G. W. Swift, A thermoacoustic stirling heat engine, *Nature*, 399 (6734) (1999) 335-338.

[4] M. Tijani and S. Spoelstra, A high performance Thermoacoustic engine, *Journal of Applied Physics*, 110 (9) (2011) 093519.

[5] De Waele, P. P. Steijaert and J. Gijzen, Thermodynamical aspects of pulse tubes, *Cryogenics*, 37 (6) (1997) 313-324.

[6] De Waele, P. Steijaert and J. Koning, Thermodynamical aspects of pulse tubes II, *Cryogenics*, 38 (3) (1998) 329-335.

[7] M. Nouh, O. Aldraihem and A. Baz, Energy harvesting of thermoacoustic-piezo systems with a dynamic magnifier, *Journal of Vibration and Acoustics*, 134 (6) (2012) 061015-1-061015-10.

[8] M. Wetzel and C. Herman, Design optimization of ther-

moacoustic refrigerators, *International Journal of Refrigeration*, 20 (1) (1997) 3-21.

[9] M. E. H. Tijani, J. C. H. Zeegers and A. De Waele, The optimal stack spacing for Thermoacoustic refrigeration, *The Journal of the Acoustical Society of America*, 112 (1) (2002) 128-133.

[10] K. Tang, G. Chen, T. Jin, R. Bao and X. Li, Performance comparison of Thermoacoustic engines with constant-diameter resonant tube and tapered resonant tube, *Cryogenics*, 46 (10) (2006) 699-704.

[11] R. Bao, G. Chen, K. Tang, Z. Jia and W. Cao, Influence of resonance tube geometry shape on performance of Thermoacoustic engine, *Ultrasonics*, 44 (2006) 1519-1521.

[12] V. Gusev, S. Job, H. Bailliet, P. Lotton and M. Bruneau, Acoustic streaming in annular thermoacoustic prime-movers, *Journal of the Acoustical Society of America*, 108 (3) (2000) 934-945.

[13] G. W. Swift, D. Gardner and S. Backhaus, Acoustic recovery of lost power in pulse tube refrigerators, *Journal of the Acoustical Society of America*, 105 (2) (1999) 711-724.

[14] M. Miwa, T. Sumi, T. Biwa, Y. Ueda and T. Yazaki, Measurement of acoustic output power in a traveling wave engine, *Ultrasonics*, 44 (2006) 1527-1529.

[15] M. Faraday, On a peculiar class of acoustical figures; and on certain forms assumed by groups of particles upon vibrating elastic surface, Philosophical Transactions of the Royal Society of London, 121 (1831) 299-340.

[16] L. Rayleigh, On the circulation of air observed in Kundt's tubes, and on some allied acoustical problems, Philosophical Transactions of the Royal Society of London, 175 (1884) 1-21.

[17] P. Westervelt, The theory of steady rotational flow generated by a sound field, *Journal of the Acoustical Society of America*, 25 (1) (1953) 60-67.

[18] W. Nyborg, Acoustic streaming, *Physical Acoustics*, 2 (Part B) (1965) 265-331.

[19] E. N. C. Andrade, On the circulations caused by the vibration of air in a tube, *Proceedings of the Royal Society of London Series A*, 134 (824) (1931) 445-470.

[20] M. Arroyo and C. Greated, Stereoscopic particle image velocimetry, *Measurement Science and Technology*, 2 (12) (1991) 1181-250 1186.

[21] M. Thompson and A. Atchley, Simultaneous measurement of acoustic and streaming velocities in a standing wave using laser Doppler anemometry, *The Journal of the Acoustical Society of America*,117 (4) (2005) 1828-1838.

[22] M. Thompson, A. Atchley and M. Maccarone, Influences of a temperature gradient and fluid inertia on acoustic streaming in a standing wave, *The Journal of the Acoustical Society of America*, 117 (4) (2005) 1839-1849.

[23] S. Moreau, H. Bailliet and J. Valière J, Measurements of inner and outer streaming vortices in a standing waveguide using laser Doppler velocimetry, *Journal of the Acoustical Society of America*, 123 (2) (2008) 640-647.

[24] S. Moreau, H. Bailliet and J. Valière, Effect of a stack on Rayleigh streaming cells investigated by laser Doppler velocimetry for application to Thermoacoustic devices, *The Journal of the Acoustical Society of America*, 125 (6) (2009) 3514-3517.

[25] Desjouy, G. Penelet, P. Lotton and J. Blondeau, Measurement of acoustic streaming in a closed-loop traveling wave resonator using laser Doppler velocimetry, *Journal of the Acoustical Society of America*, 126 (5) (2009) 2176-2183.

[26] T. Biwa, Y. Tashiro, M. Ishigaki, Y. Ueda and T. Yazaki, Measurements of acoustic streaming in a looped-tube Thermoacoustic engine with a jet pump, *Journal of Applied Physics*, 101 (6) (2007) 064914-064914.

[27] P. Debesse, Vers une mesure du vent thermoacoustique, Ph.D. thesis, Université Pierre et Marie Curie-Paris VI (2008).

[28] G. W. Smith and G. W. Swift, Measuring second-order time-average pressure, *The Journal of the Acoustical Society of America* (2001) 110:717.

[29] B. Ward, J. Clark and G. W. Swift, Design environment for low-amplitude Thermoacoustic energy conversion, DeltaEC version 6.2: Users guide (2008).

[30] R. Paridaens, S. Kouidri and F. Jebali Jerbi, Investigation on the generation mechanisms of acoustic streaming in a thermoacoustic prime mover, Cryogenics, 58 (2013) 78-84.

[31] M. Hamilton, Y. Ilinskii and E. Zabolotskaya, Acoustic streaming generated by standing waves in two-dimensional channels of arbitrary width, *Journal of the Acoustical Society of America* (2003) 113-153.

[32] R. Paridaens, S. Kouidri and F. J. Jerbi, Dc flow investigations in thermoacoustic prime mover, *ASME 2011 International Mechanical Engineering Congress and Exposition*, American Society of Mechanical Engineers (2011) 439-444.